JOURNAL OF GEOPHYSICAL RESEARCH, VOL. 112, F02011, doi:10.1029/2005JF000376, 2007

Click Here for Full Article

Modeling the effect of nonuniform sediment on the dynamics of offshore tidal sandbanks

Pieter C. Roos,[1] Rik Wemmenhove,[2] Suzanne J. M. H. Hulscher,[1]
Harry W. M. Hoeijmakers,[3] and N. P. Kruyt[3]

Received 20 July 2005; revised 5 October 2006; accepted 22 November 2006; published 3 May 2007.

[1] Tidal sandbanks are large-scale bed features present in many shallow shelf seas. Here we investigate the effect of nonuniform sediment on their dynamics, with a particular aim to explain observed surficial grain size variations over tidal sandbanks from a process-based modeling perspective. To this end, we use a linear stability analysis that describes the positive feedback mechanism between hydrodynamics, sediment, and the seabed responsible for sandbank formation on a horizontal shelf. In this model the sediment transport and bed evolution modules are extended by introducing an active layer and a bimodal sediment mixture. We include a dynamic hiding/exposure description of sediment transport, enhancing the transport of coarse grains and inhibiting the transport of finer grains. The model results show that for symmetrical tidal conditions, coarse grains tend to accumulate at the bank crests. Moreover, the growth rates of the perturbations increase compared to the case of uniform sediment, while the preferred wavelength and bank orientation remain unchanged. For asymmetrical tidal conditions we find a spatial phase shift between topography and the mean grain size fraction, indicating an accumulation of coarse grains on the lee side of the bank. The model results qualitatively agree with observations from banks on the Belgian continental shelf.

Citation: Roos, P. C., R. Wemmenhove, S. J. M. H. Hulscher, H. W. M. Hoeijmakers, and N. P. Kruyt (2007), Modeling the effect of nonuniform sediment on the dynamics of offshore tidal sandbanks, *J. Geophys. Res.*, *112*, F02011, doi:10.1029/2005JF000376.

1. Introduction

[2] Shallow shelf seas, like the North Sea, exhibit a variety of rhythmic bed forms. The largest of these patterns are tidal sandbanks, with a wavelength of 5–10 km, a height up to tens of meters and an oblique orientation with respect to the tidal current [*Dyer and Huntley*, 1999]. Tidal sandbanks are dynamic features that play an important role in sea use. They protect the coast from wave action, serve as source of hydrocarbons and sand, may interfere with navigation, and act as nursery ground for fish. Insight in sandbank dynamics is of benefit to the sustainable use of coastal seas.

[3] The occurrence of tidal sandbanks has been explained as a morphodynamic instability of a horizontally flat seabed in an offshore environment, subject to tidal flow and bed load sediment transport [*Huthnance*, 1982; *De Vriend*, 1990; *Hulscher et al.*, 1993]. The underlying hydrodynamic mechanism, known as tidal rectification, describes how tidal currents are deflected by tide-topography interactions [*Zimmerman*, 1982]. This approach leads to preferred values of wavelength and bank orientation, in agreement with observations. A typical feature of these idealized morphodynamic models is the assumption of a uniform sediment size.

[4] However, observations in, for example, the North Sea indicate a significant pattern of surficial grain size variations over tidal sandbanks (see Table 1 and references cited therein). Concentrations of coarse grains are found either at the crest of the ridges, or on the lee side of the ridges. These patterns particularly apply to the well-documented examples on the Belgian continental shelf, such as Baland Bank, Nieuwpoort Bank, Stroombank, Broers Bank, Middelkerke Bank, Kwinte Bank and Hinderbank. Observations at other locations are not so conclusive, for example showing an opposite pattern with fine sediment at the crest, or a pattern that is hard to interpret due to grain size variations in the along-bank direction (Table 1).

[5] Most of the knowledge on the processes related to sandbank dynamics is based on strongly simplified models, in which uniform sediment is assumed. Clearly, these models are unable to describe and explain spatial grain size variations over tidal sandbanks. Besides, it is unclear whether the inclusion of nonuniform sediment affects the topographic bank characteristics (wavelength, orientation, growth and migration rates) obtained with the existing models.

[1] Water Engineering and Management, Faculty of Engineering Technology, University of Twente, Enschede, Netherlands.
[2] Computational Mechanics and Numerical Mathematics, Institute of Mathematics and Computing Science, University of Groningen, Groningen, Netherlands.
[3] Engineering Fluid Dynamics, Faculty of Engineering Technology, University of Twente, Enschede, Netherlands.

Copyright 2007 by the American Geophysical Union.
0148-0227/07/2005JF000376$09.00

Table 1. Overview of Observed Grain Size Variations Over Tidal Sandbanks

Location	Qualitative Observations and References	Mean Grain Sizes, μm
Sizewell-Dunwich Banks (UK)	coarsest sediment on steeper landward flank; seasonal variations in surficial sediment distribution; also cohesive sediments and along-bank variations [*Lees*, 1983]	100–200
Kwinte Bank (Belgium)	fine and well-sorted sediment on landward flank; coarser sediment with poorer sorting on seaward flank [*Gao et al.*, 1994][a]	200–700
Middelkerke Bank (Belgium)	coarsest sand near crest, seaward at the northern end and landward at southern end [*Trentesaux et al.*, 1994; *Trentesaux et al.*, 1999]; storms cause a coarsening on the seaward flank and a fining on the landward flank [*Houthuys et al.*, 1994].	200–800
Georges Bank (Gulf of Maine, US)	sand and gravelly sediment in shallower parts; silty or clayey sand in deeper parts [*Hastings et al.*, 2000]	not readily available
Westhinder Bank (Belgium)	coarsest sediment on crests and west of the stoss slope; also along-bank gradients near "kink"; fine sediments at kink's stoss slope [*Deleu et al.*, 2004]	250–400
Broers Bank (Belgium)	coarsening toward bathymetric highs; swales contain high percentage of silt [*Van Lancker et al.*, 2000]	150–500
Baland Bank, Nieuwpoort Bank, Stroombank (Belgium)	coarsest sediment on steep landward flanks; finest sediment on gentle seaward flanks; better sorting on steep flanks [*Van Lancker*, 1999][a]	250–450[b], 150–350[c]

[a]By definition, the degree of 'sorting' is directly related to the standard deviation σ_ϕ (as introduced in section 2.2): "well sorted" denotes a small σ_ϕ, and "poorly sorted" denotes a larger σ_ϕ.
[b]Baland Bank.
[c]Nieuwpoort Bank and Stroombank.

[6] Using a process-based stability approach, *Walgreen et al.* [2004] recently investigated the effect of graded sediment on tidal sandbanks, but in a geometric context different from the one introduced above. Their approach is based on the morphodynamic model by *Calvete et al.* [2001], which distinguishes a horizontal outer shelf, a linearly sloping inner shelf and a shoreface. Depending on the hydrodynamic conditions and the dominant mode of transport, the inner shelf develops features known as shoreface-connected sand ridges (with storms, suspended load transport) and tidal sandbanks (with tidal flow, bed load transport). Focusing on the latter, *Walgreen et al.* [2004] considered a bimodal sediment mixture, subject to dynamic hiding/exposure in an active layer model [*Hirano*, 1971; see also *Ribberink*, 1987; *Seminara*, 1995]. Their results show, for symmetrical tidal conditions, a coarsening at the bank crests and a fining in the troughs. Tidal asymmetry causes the peak in mean grain size to shift in the direction of the residual sediment flux, with the coarsest material accumulating on the lee side. Their results further indicate an increase in growth and migration rate for a bimodal mixture, while the wavelength remains unchanged. For shoreface-connected sand ridges, *Walgreen et al.* [2003] earlier found agreement between observations and results from a dynamic hiding model.

[7] The goal of this paper is twofold. First, we show that most of the observed grain size variations can be explained by an active layer model with a bimodal sediment mixture and a dynamic hiding/exposure formulation, incorporated in the existing stability models for tidal sandbank formation in an offshore environment [*Huthnance*, 1982; *De Vriend*, 1990; *Hulscher et al.*, 1993]. A second objective is to find out whether the banks on a sloping inner shelf bounded by a shoreface [*Walgreen et al.*, 2004] and the banks in our fully offshore model are consistent in terms of bank dynamics and grain size variations (for a sketch of the two model geometries, see Figure 1). In our offshore case, we do not encounter the complications of the cross-shore structure induced by shoreface and inner shelf [*Walgreen et al.*, 2004]. This simplifies our analysis and allows us to investigate the system in some more mathematical detail.

[8] This paper is organized as follows. The morphodynamic model, following a linear stability approach, is presented in section 2. Next, in section 3, we present the results, distinguishing between symmetrical and asymmetrical tidal conditions. In section 4 we discuss the physical interpretation of the results, along with their relation to the work by *Walgreen et al.* [2004] as well as observations. Finally, section 5 contains the conclusion and recommendations for further research.

2. Model

[9] The chosen modeling approach, known as stability analysis (for a review of stability methods used in coastal morphodynamics, see *Dodd et al.* [2003]), focuses on the

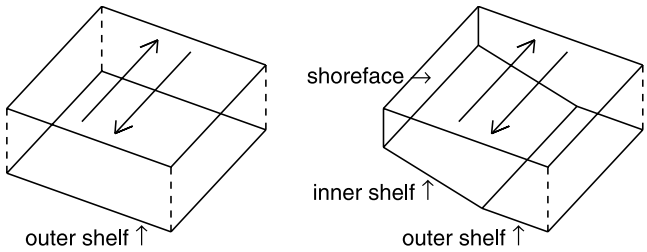

Figure 1. Two model geometries for tidal sandbanks. (left) Offshore model of the present study. (right) Shelf model with shoreface, sloping inner shelf, and horizontal outer shelf [*Calvete et al.*, 2001; *Walgreen et al.*, 2004]. The arrows indicate the direction of the tidal flow.

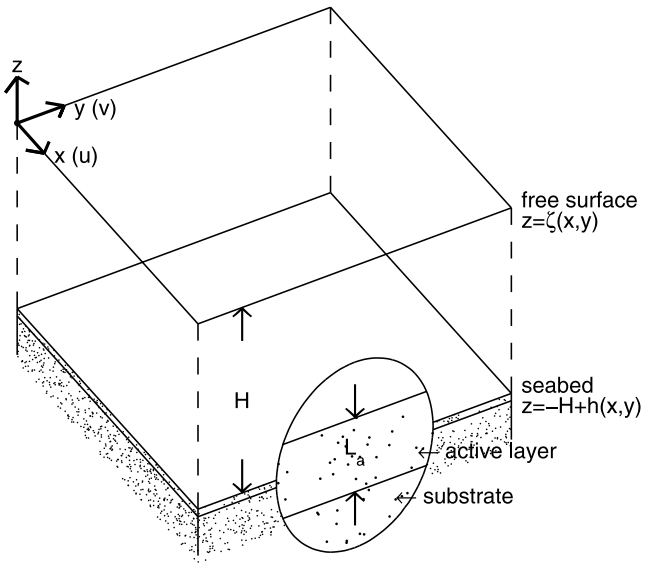

Figure 2. Definition sketch of the model geometry, including a close-up of the seabed showing the active layer and the substrate.

formation stage of tidal sandbanks [*Huthnance*, 1982; *De Vriend*, 1990; *Hulscher et al.*, 1993]. Typically, these models describe the growth or decay of topographic perturbations to the reference situation of a flat seabed, termed the ''basic state.'' The perturbation with the largest growth rate, the ''fastest growing mode,'' is the bank pattern assumed to be dominant in reality. The corresponding wavelength, orientation and migration rate can thus be compared with observations. By including an active layer and graded sediment, our model results additionally describe the surficial grain size distribution over tidal sandbanks. Below we introduce the morphodynamic model, with emphasis on the geometry and the active layer, the description of a nonuniform sediment mixture, the hiding/exposure formulation, the hydrodynamics and the solution method.

2.1. Geometry and Active Layer

[10] We consider an offshore domain of average depth H ($\sim$25 m), far away from coastal boundaries (Figure 2). We introduce a three-dimensional coordinate system with horizontal coordinates $\boldsymbol{x} = (x, y)$. The vertical axis points upward, with the free surface level at $z = \zeta(\boldsymbol{x})$ and the bottom level at $z = -H + h(\boldsymbol{x})$. The depth-averaged flow velocity vector $\boldsymbol{u}$ consists of two components u and v, in x and y directions, respectively. The oscillatory tidal flow, with typical maximum current velocities of $U \sim 1$ m s^{-1}, will be specified in section 2.4.

[11] Following the active layer approach [*Hirano*, 1971; see also *Ribberink*, 1987; *Seminara*, 1995], we assume that the seabed consists of two layers: an active layer and a substrate (Figure 2). Sediment particles in the active layer are in interaction with the flow, whereas particles in the underlying substrate layer are not. The active layer is well mixed and has a thickness L_a. To account for the presence of sand ripples (typical height of the order of a centimeters), the thickness of the active layer L_a is taken of the order of a few centimeters.

2.2. Nonuniform Sediment

[12] The sediment in the seabed consists of grains of different sizes d. Grain sizes are commonly expressed in terms of the so-called phi scale, given by

$$\phi = -\log_2 (d/d_{\mathrm{ref}}), \quad \text{with} \quad d_{\mathrm{ref}} = 1 \text{ mm}, \tag{1}$$

as the ϕ values of sediment usually follow a normal (i.e., Gaussian) distribution [*Dyer*, 1986]. The sediment is thus characterized by a mean value μ_ϕ and a standard deviation σ_ϕ. In addition, the skewness Sk_ϕ is a measure for the preferential spread to one side of the average [*Blott and Pye*, 2001]; it is zero for a purely normal distribution. On the basis of the mean μ_ϕ, the quantity $d_{\mathrm{m}} \equiv d_{\mathrm{ref}} 2^{-\mu_\phi}$ is defined as the mean diameter.

[13] To represent such a nonuniform sediment mixture in a convenient way, we introduce a finite number of grain sizes $d^{(j)}$ with associated volume fraction $F^{(j)}$. These fractions may vary in both space and time, but the sum of all grain size fractions must equal one everywhere: $\Sigma_j F^{(j)} = 1$.

[14] Within the active layer, each grain size class j should satisfy sediment continuity. This conservation law relates local changes in both bed level and grain size distribution to the divergence of the tidally averaged sediment flux $\langle \boldsymbol{q}_{\mathrm{b}}^{(j)} \rangle$ of class j (in m^2 s^{-1}) [*Walgreen et al.*, 2003]:

$$(1-p)\left[F^{(j)} \frac{\partial h}{\partial t} + L_{\mathrm{a}} \frac{\partial F^{(j)}}{\partial t}\right] + \boldsymbol{\nabla} \cdot \langle \boldsymbol{q}_{\mathrm{b}}^{(j)} \rangle = 0. \tag{2}$$

This formulation, in which the interaction between the active layer and the substrate is neglected, is actually a special case of a more general formulation [*Walgreen et al.*, 2003]. In the initial stage of formation, sorting can be seen as the rearrangement of material in the active layer with negligible interaction between substrate and active layer [*Ribberink*, 1987; *Seminara*, 1995]. In equation (2), p is the bed porosity (assumed constant: $\sim$0.4), $\boldsymbol{\nabla} = (\partial/\partial x, \partial/\partial y)$ is the horizontal nabla operator and angle brackets $\langle \cdot \rangle$ denote tidal averaging. Considering the tidal average of the sediment flux is justified since the timescale on which the seabed evolves (decades to centuries) is much larger than the tidal cycle (12.42 h).

[15] By summing over all grain size fractions, the individual sediment continuity equations (2) add up to a single equation relating the bed evolution to the divergence of the total sediment flux:

$$(1-p)\frac{\partial h}{\partial t} + \boldsymbol{\nabla} \cdot \left[\sum_j \langle \boldsymbol{q}_{\mathrm{b}}^{(j)} \rangle\right] = 0. \tag{3}$$

Next, eliminating the bed evolution $\partial h/\partial t$ from equations (3) and (2) leads to evolution equations of the individual grain size fractions $F^{(j)}$.

[16] To keep the model as transparent as possible, we consider a bimodal sediment mixture consisting of two grain sizes: coarse grains d^{co} with fraction F^{co} and fine grains d^{fi} with fraction F^{fi}. Such a sediment mixture is fully characterized by three parameters: the mean grain diameter d_{m}, the standard deviation σ_ϕ and the coarse grain fraction F^{co} (see Appendix A). The assumption of a bimodal mixture

allows us to describe spatial variations in mean grain size, sorting (i.e., the standard deviation σ_ϕ) and skewness (see the expressions in Appendix A).

2.3. Dynamic Hiding/Exposure Formulation

[17] Considering conditions in a tide-dominated offshore environment, we assume that sediment is transported mainly as bed load. For a given grain size class j, the bed load sediment flux $\boldsymbol{q}_b^{(j)}$ (in $m^2\ s^{-1}$) is modeled as

$$q_b^{(j)} = F^{(j)} G^{(j)} q_b^{\mathrm{ref}}. \tag{4}$$

Here $F^{(j)}$ is the grain size fraction and $\boldsymbol{q}_b^{\mathrm{ref}}$ a reference sediment flux that corresponds to the situation in which the sediment were uniform with grain size d_m; $\boldsymbol{q}_b^{\mathrm{ref}}$ will be specified below. Furthermore, $G^{(j)}$ is a dimensionless dynamic hiding/exposure coefficient, given by

$$G^{(j)} = \left(\frac{d^{(j)}}{d_m}\right)^{c_b}, \tag{5}$$

with positive power c_b ($\sim$0.75) [*Walgreen et al.*, 2003]. The transport of fine grains is hindered as they are protected from movement by the surrounding coarser grains (hiding if $d^{(j)} < d_m$). Conversely, the transport of coarse grains is enhanced as, in the presence of finer grains, they are more exposed and thus transported more easily by the flow (exposure if $d^{(j)} > d_m$). It is worthwhile pointing out that the adopted hiding/exposure formulation, as given by equation (5), reflects the qualitative properties of the hiding/exposure mechanism.

[18] The reference bed load sediment flux $\boldsymbol{q}_b^{\mathrm{ref}}$ (in $m^2\ s^{-1}$) in equation (4) follows from a transport formula:

$$\boldsymbol{q}_b^{\mathrm{ref}} = \nu_b |\boldsymbol{u}|^3 \left(\frac{\boldsymbol{u}}{|\boldsymbol{u}|} - \lambda_b \nabla h\right). \tag{6}$$

This is a standard velocity power law with coefficient ν_b and a gravitational bed slope effect with dimensionless coefficient λ_b (for parameter values, see Table 2). We neglect the threshold for sediment motion, as this does not affect the results qualitatively [see, e.g., *Hulscher et al.*, 1993].

[19] In the case of uniform sediment, there is effectively only one grain size $d^{(j)} = d_m$, so $F^{(j)} = 1$ and equation (5) becomes $G^{(j)} = 1$. For uniform sediment, the transport formulation (4) thus reduces to $\boldsymbol{q}_b^{(j)} = \boldsymbol{q}_b^{\mathrm{ref}}$, as used in earlier models [see, e.g., *Hulscher et al.*, 1993].

2.4. Hydrodynamics and Basic Flow

[20] The water motion is described by the depth-averaged shallow water equations in two horizontal dimensions [see, e.g., *Hulscher et al.*, 1993]:

$$g\nabla\zeta + \frac{\partial \boldsymbol{u}}{\partial t} + (\boldsymbol{u}\cdot\nabla)\boldsymbol{u} + f\boldsymbol{e}_z \times \boldsymbol{u} + \frac{r\boldsymbol{u}}{H-h} = 0, \tag{7}$$

$$\nabla\cdot[(H-h)\boldsymbol{u}] = 0. \tag{8}$$

Here g is the acceleration of gravity, $f = 2\Omega\sin\theta$ is a Coriolis parameter (where $\Omega = 7.292 \times 10^{-5}$ rad s^{-1} is the angular frequency of the Earth's rotation and θ is the latitude) and $\boldsymbol{e}_z$ is the unit vector in z direction. Moreover, r is a coefficient of linear bottom friction that follows from Lorentz's linearization of a quadratic friction law [*Zimmerman*, 1982]. We apply the rigid lid approach, which implies that the contribution of the free surface elevation ζ to the water depth in the friction term and continuity equation is neglected. Finally, the quasi-stationary approach implies that the bed can be treated as stationary on the tidal timescale, so the term $\partial h/\partial t$ does not need to be included in the continuity equation (8). Parameter values are listed in Table 2.

[21] The stability approach requires an exact and physically meaningful solution to the set of model equations, termed the basic state [*Dodd et al.*, 2003]. The model introduced above indeed allows for such a solution: one that represents a spatially uniform yet time-dependent flow $\boldsymbol{u}_0(t) = (u_0(t), v_0(t))$ over a flat seabed of uniform depth H (i.e. $h_0 = 0$). This basic flow is forced by a horizontal pressure gradient $\nabla\zeta_0$. We choose the basic flow to represent an oscillatory tidal flow in the x direction, according to

$$u_0(t) = U_{M_0} + U_{M_2}\cos\sigma t + U_{M_4}\cos(2\sigma t - \beta), \tag{9}$$

and $v_0 = 0$. The main component is a semidiurnal lunar M_2 tide of angular frequency σ ($\sim 1.41 \times 10^{-4}$ rad s^{-1}) and with a velocity amplitude U_{M_2} (typically $\sim$1 m s^{-1}). The two other terms in equation (9) allow us to introduce asymmetry in the tidal forcing: a residual current U_{M_0} and an M_4 component of angular frequency 2σ, with amplitude U_{M_4} and a temporal phase shift β with respect to the M_2 component.

[22] Assuming that also the grain size fractions F_0^{co} and F_0^{fi} are spatially uniform, the sediment transport is spatially uniform as well. This means that the divergence of the sediment flux vanishes everywhere in the domain, so, according to equation (3), the flat seabed remains flat. The basic state serves as a starting point for the stability approach introduced below.

2.5. Stability Approach and Solution Method

[23] As noted in the Introduction, tidal sandbanks can be considered as morphological instabilities of a flat seabed [*Huthnance*, 1982; *De Vriend*, 1990; *Hulscher et al.*, 1993]. To model this, we consider the state of the system relative to the basic state introduced in section 2.4. We symbolically write the state of the system as $\psi = (h, \boldsymbol{u}, \zeta, L_a, F^{\mathrm{co}}, F^{\mathrm{fi}}, G^{\mathrm{co}}, G^{\mathrm{fi}}, \boldsymbol{q}_b^{\mathrm{co}}, \boldsymbol{q}_b^{\mathrm{fi}}, \boldsymbol{q}_b^{\mathrm{ref}}, d_m, \sigma_\phi)$, including the bimodal sediment characteristics and the hiding/exposure mechanisms. Next, we expand the state about the basic state ψ_0, i.e.,

$$\psi = \psi_0 + \epsilon\psi_1 + O(\epsilon^2). \tag{10}$$

The perturbed state ψ_1 consists of the perturbed components of each of the system's state variables. The dimensionless expansion parameter ϵ quantifies the extent to which the perturbed state differs from the basic state, topographically or in terms of grain size fractions. It is assumed to be small, such that higher-order contributions to ψ can be neglected. Now introduce wavy bottom perturbations of the form

$$h_1(x,y,t) = \hat{h}(t)\exp(i\boldsymbol{k}\cdot\boldsymbol{x}) + \text{c.c.}, \tag{11}$$

characterized by a complex amplitude $\hat{h}(t)$ and a topographic wave vector $\boldsymbol{k} = (k, \ell)$. The latter determines the

Table 2. Physical Parameters, Tidal Conditions I–III, and Properties of the Fastest Growing Mode for Uniform Sediment

Description and Symbol	Value(s)	Dimension
Physical Parameters		
Mean water depth H	25	m
Latitude θ	50.5	°N
Coriolis parameter f	1.13×10^{-4}	s^{-1}
Friction coefficient r	2.5×10^{-3}	m s^{-1}
Transport coefficient ν_b	1.0×10^{-5}	m^{-1} s^2
Bed slope coefficient λ_b	1.0	
Mean grain diameter d_{m0}	0.25	mm
Bed porosity p	0.40	
Hiding power c_b	0.50–0.75	
Tidal Conditions [a,b]		
Residual current U_{M0}	0.00, 0.05, 0.00	m s^{-1}
M_2 component U_{M2}	1.00, 1.00, 1.00	m s^{-1}
M_4 component U_{M4}	0.00, 0.00, 0.05	m s^{-1}
M_4 phase β (w.r.t. M_2)	-, -, 0	rad
Properties of the fgm [a,c]		
Wavelength L_{fgm}^{ref}	6.6, 6.7, 6.6	km
Bank orientation ϑ_{fgm}^{ref} [d]	31, 31, 31	degrees
Growth time $(\omega_{fgm,r}^{ref})^{-1}$	2.6, 2.6, 2.6	10^2 yr
Migration speed $c_{mig,fgm}^{ref}$	0.0, 0.4, 0.2	m yr^{-1}

[a]For tidal conditions and properties of fgm, the first value is for tidal condition I, the second is for tidal condition II, and the third is for tidal condition III.
[b]Basic flow parameters; see equation (9).
[c]Fastest growing mode for uniform sediment.
[d]Counterclockwise angle between basic flow and bank crest.

wavelength $L = 2\pi/|\boldsymbol{k}|$ of the bottom perturbation as well as its orientation ϑ with respect to the tidal flow direction ($\tan\vartheta = \ell/k$). Moreover, c.c. denotes complex conjugation.

[24] For all perturbed state variables, we assume a spatial structure similar to that of the bottom perturbation (11). For example, the perturbed coarse grain fraction is given by

$$F_1^{co}(x,y,t) = \hat{F}(t)\exp(i\boldsymbol{k}\cdot\boldsymbol{x}) + \text{c.c.}, \tag{12}$$

with complex amplitude $\hat{F}(t)$. The perturbed hydrodynamic quantities are solved from the set of equations (2)–(8), after linearizing with respect to ϵ. The hydrodynamic part of the solution involves a truncated harmonic expansion in time to account for the generation of higher harmonics as a result of tide-topography interactions [*Zimmerman*, 1981]. The hydrodynamic solution then leads to a perturbed sediment transport pattern of both coarse and fine grains during the tidal cycle. The tidal average of the sediment transport in turn determines the evolution of the seabed and the grain size fractions. These dynamics are expressed in a set of coupled linear evolution equations for the complex amplitudes $\hat{h}$ and $\hat{F}$, to be presented in section 3.1. Further details of the solution method are given in Appendix B.

3. Results

3.1. Set of Evolution Equations

[25] Considering the general case of bimodal sediment, we find the following set of coupled evolution equations for the amplitudes of the sandbank profile $\hat{h}$ and the coarse grain fraction perturbation $\hat{F}$:

$$\begin{bmatrix} \partial\hat{h}/\partial t \\ L_{a0}\partial\hat{F}/\partial t \end{bmatrix} = \begin{bmatrix} P\omega^{ref} & ikQ\langle q_{b0,x}^{ref}\rangle \\ R\omega^{ref} & ikS\langle q_{b0,x}^{ref}\rangle \end{bmatrix} \begin{bmatrix} \hat{h} \\ \hat{F} \end{bmatrix}. \tag{13}$$

Here L_{a0} is the active layer thickness in the basic state. Equation (13) describes the simultaneous evolution of both topography (slowly) and grain size distribution (adapting more quickly). The coefficients P, Q, R and S, all real-valued and related to the sediment characteristics, are given by

$$P = F_0^{co}G_0^{co} + F_0^{fi}G_0^{fi} > 1, \tag{14}$$

$$Q = \frac{1}{1-p}\left(P\,T - \left[G_0^{co} - G_0^{fi}\right]\right), \tag{15}$$

$$R = F_0^{co}F_0^{fi}\left(G_0^{co} - G_0^{fi}\right) > 0, \tag{16}$$

$$S = \frac{1}{1-p}\left(R\,T - \left[F_0^{co}G_0^{fi} + F_0^{fi}G_0^{co}\right]\right), \tag{17}$$

with $T = c_b\sigma_{\phi 0}\ln 2/\sqrt{F_0^{co}F_0^{fi}} > 0$, as given in equation (B7) in Appendix B. The quantity ω^{ref} is termed the reference growth rate; it denotes the growth rate that would be obtained for uniform sediment, with a grain size equal to the mean grain size d_m of the bimodal mixture. Furthermore, $\langle \boldsymbol{q}_{b0,x}^{ref}\rangle$ is the tidally averaged sediment flux of such uniform sediment over a flat bed, i.e., in the basic state. Both ω_{ref} and $\langle \boldsymbol{q}_{b0,x}^{ref}\rangle$ are specified in Appendix B.

[26] The proof that $P > 1$ follows immediately from the following two observations: (1) $P = 1$ for $\sigma_{\phi 0} = 0$ (the trivial case in which the coarse and fine grains are identical) and (2) $\partial P/\partial\sigma_{\phi 0} = TR/\sigma_{\phi 0} > 0$. Furthermore, we find $R > 0$ because hiding/exposure enhances the transport of coarse grains and inhibits the transport of fine grains: $G_0^{co} > G_0^{fi}$. The signs of Q and S are not known a priori. It should be noted that in general $S < 0$, except for unrealistic mixtures containing an extremely small fraction of very fine grains.

3.2. Properties of the Solution

[27] The solution to (13) can be found analytically, but it is not transparent and hence hard to interpret. In this section, we derive the properties of the solution that are of main interest: asymptotic values of the growth and the grain size variations over the bank profile. We start with the latter.

[28] The spatial phase shift χ between topography and coarse grain fraction is of particular interest, as it shows the location on the tidal sandbank where the coarse grains are concentrated (Figure 3).

[29] It is given by

$$\chi = \arg(\bar{\xi}), \qquad \text{where} \qquad \xi = \hat{F}/\hat{h}, \tag{18}$$

and an overbar denotes complex conjugation. The complex quantity ξ can be interpreted as the relative fraction amplitude: its absolute value not meaningful in a linear stability analysis, its argument representing the spatial phase shift as introduced above. From equation (13), an evolution equation for ξ can be derived and solved, leading to asymptotic values of ξ and hence of χ. The relative fraction amplitude ξ obeys the following evolution equation, quadratic in ξ:

$$L_{a0}\frac{\partial\xi}{\partial t} = -L_{a0}ikQ\langle q_{b0,x}\rangle\xi^2 + \left[ikS\langle q_{b0,x}\rangle - L_{a0}P\omega^{ref}\right]\xi + R\omega^{ref}. \tag{19}$$

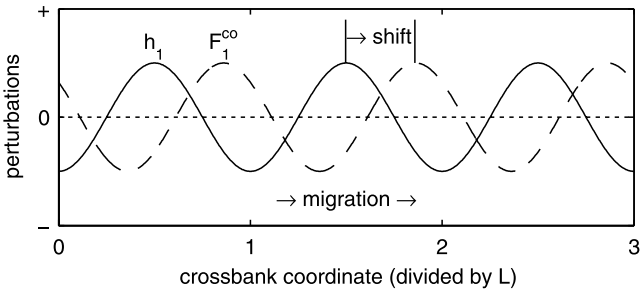

Figure 3. Sketch of the bottom perturbation h_1 (solid curve) and the coarse-grain fraction perturbation F_1^{co} (dashed curve), plotted against the cross-bank coordinate (scaled by wavelength $L = 2\pi/|\boldsymbol{k}|$). The spatial phase shift χ is positive when h_1 lags F_1^{co} (here $\chi = 130$), in the direction of migration (i.e., the direction of the residual sediment flux).

[30] The solution can be found analytically and reads

$$\xi(t) = \frac{\xi_+\xi_-\left[\exp\left(\sqrt{D}t/L_{a0}\right) - 1\right]}{\xi_- \exp\left(\sqrt{D}t/L_{a0}\right) - \xi_+}, \tag{20}$$

where

$$\xi_\pm = \frac{ikS\langle q_{b0,x}\rangle - L_{a0}P\omega^{ref} \pm \sqrt{D}}{2L_{a0}ikQ\langle q_{b0,x}\rangle}, \tag{21}$$

$$D = \left[ikS\langle q_{b0,x}\rangle - L_{a0}P\omega^{ref}\right]^2 + 4L_{a0}ikQ\langle q_{b0,x}\rangle R\omega^{ref}, \tag{22}$$

and we have taken $\xi(0) = 0$. Because $\mathrm{Re}(\sqrt{D}/L_{a0}) > 0$, it follows that $\lim_{t\to\infty} \xi = \xi_+$. The value ξ_+ thus determines the asymptotic value of the spatial phase shift between topography and coarse grain fraction, whereas ξ_- has no physical importance.

[31] The seabed then evolves according to

$$\frac{\partial \hat{h}}{\partial t} = \omega\hat{h}, \qquad \text{with} \qquad \omega = P\omega^{ref} + ikQ\langle \boldsymbol{q}^{ref}_{b0,x}\rangle\xi. \tag{23}$$

This is exponential growth (or decay), with complex growth rate ω. Its real part ω_r is related to the amplitude evolution of the perturbation, with positive values indicating growth and negative values indicating decay. The imaginary part is associated with the migration of the bottom waviness, the migration speed being given by

$$c_{mig} = \frac{-\omega_i}{|\boldsymbol{k}|}. \tag{24}$$

Within a stability approach, the so-called fastest growing mode is of particular interest. As noted at the beginning of section 2, the fastest growing mode is the perturbation for which ω_r attains its maximum. The corresponding topographic wave number $\boldsymbol{k}_{fgm} = (k_{fgm}, \ell_{fgm})$ characterizes the tidal sandbank that is most likely to emerge from a randomly perturbed seabed. The properties of the fastest growing mode (wavelength, orientation, migration speed, location of coarse grain concentration) are the principal output of the model: this is the information to be compared with observations. As a consequence of considering nonuniform sediment, the location of coarse (and fine) grains relative to the bank profile now appears as a new model result.

[32] To interpret the solution to (13), we distinguish different situations: (1) the reference case of uniform sediment (below), (2) bimodal mixture with symmetrical tide (section 3.3), (3) bimodal mixture with asymmetrical tide (section 3.4). In the latter case, which is the most realistic one, *Walgreen et al.* [2004] used an approximation for the solution to equation (13), which we will compare with our more general solution.

[33] In the reference case of uniform sediment, our model reduces to the existing model for uniform sediment. In that case, there is effectively only one grain size ($d^{co} = d_{m0}$, $\sigma_{\phi 0} = 0$), so $F^{co} = 1$, which implies that the perturbed grain size fraction vanishes, i.e., $\hat{F} = 0$ and $\xi = 0$. Furthermore, in that case $P = 1$ so the exponential growth in equation (23) indeed reduces to the reference growth rate for uniform sediment: $\omega = \omega^{ref}$.

3.3. Symmetrical Tide

[34] For symmetrical tidal conditions, the tidally averaged reference sediment flux $\langle \boldsymbol{q}^{ref}_{b0,x}\rangle$ vanishes. From equation (23), we find exponential growth of the bottom perturbation with growth rate

$$\omega = P\omega^{ref}. \tag{25}$$

As the factor $P > 1$ only depends on the sediment properties and not on the topographic wave vector $\boldsymbol{k}$, the growth and migration rates increase by a uniform factor compared to the reference case of uniform sediment. In turn, this implies that the fastest growing mode $\boldsymbol{k}_{fgm}$ does not shift, i.e., the preferred wavelength and orientation are identical to those of the uniform case presented in section 3.1.

[35] For the spatial phase shift χ between topography and the coarse grain fraction, we find

$$\xi = \frac{R}{L_{a0}P} > 0, \qquad \text{so} \qquad \chi = 0. \tag{26}$$

Here ξ is real-valued and positive, since the active layer thickness L_{a0}, as well as the coefficients P and R are all real-valued and positive (assuming $c_b > 0$). As $\chi = 0$,there is no spatial phase shift and we conclude that coarse grains tend to accumulate at the crests, whereas finer grains gather in the troughs.

3.4. Asymmetrical Tide

[36] Now consider an asymmetrical tide such that the tidally averaged reference sediment flux $\langle \boldsymbol{q}^{ref}_{b0,x}\rangle$ is nonzero. We choose our coordinate system such that the asymmetry, and hence bank migration, is in the positive x direction, i.e., $\langle \boldsymbol{q}^{ref}_{b0,x}\rangle > 0$ and the migration speed c_{mig} is positive so, according to equation (24), the imaginary part of the growth rate is negative: $\omega_i < 0$.

[37] The asymptotic value ξ_+ in equation (21) leads to the following growth rate:

$$\omega = \frac{1}{2}P\omega^{ref} + \frac{ikS\langle q^{ref}_{b0,x}\rangle + \sqrt{D}}{2L_{a0}}, \tag{27}$$

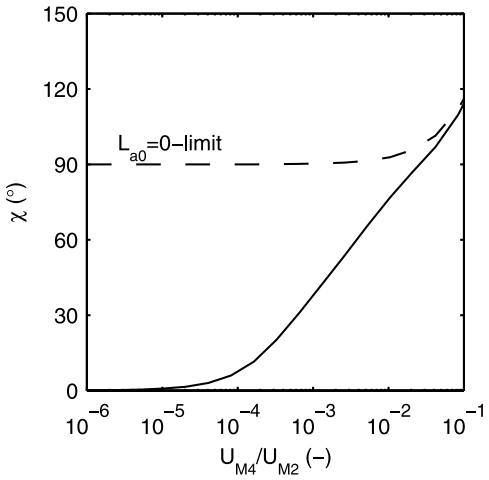

Figure 4. Spatial phase shift χ for an M_2 tide plus a small M_4 component using the exact solution (solid curve) and in the $L_{a0} = 0$ limit (dashed curve). Parameter values are $d_{m0} = 0.5$ mm, $\sigma_{\phi 0} = 2$, $F_0^{co} = 0.5$, $L_{a0} = 5$ cm, and $\beta = 0$. For the exact solution we used the topographic wave numbers of the fastest growing mode from the uniform case.

with D from equation (22). The k dependency in equation (27) suggests that the fastest growing mode $\boldsymbol{k}_{fgm}$ may shift to another value. However, it turns out that the fastest growing mode is not significantly affected in most cases. This can be seen by investigating the simplified case in which the grain size perturbation adapts instantaneously to the growing and migrating topography. This approximation corresponds to neglecting the term $L_{a0}\partial\hat{F}/\partial t$ in equation (13), i.e., to using the $L_{a0} = 0$ approximation.

[38] The growth rate then reduces to

$$\tilde{\omega} = \left(P - \frac{QR}{S}\right)\omega^{ref}. \tag{28}$$

The factor P-QR/S is independent of $\boldsymbol{k}$, so the fastest growing mode indeed does not shift. For the spatial phase shift between topography and coarse grain fraction, determining the location where coarse grains are concentrated, we find

$$\tilde{\xi} = \frac{Ri\omega^{ref}}{kS\langle q_{b0,x}^{ref}\rangle}. \tag{29}$$

As k, $\langle \boldsymbol{q}_{b0,x}^{ref}\rangle$, R and S are all real-valued, the spatial phase shift χ is fully determined by the reference growth rate and not by the details of the sediment mixture. For growing modes, we further see that $\frac{1}{2}\pi < \chi < \pi$, i.e., the peak in coarse grain fraction occurs on the lee side of the migrating bed form (as depicted in Figure 3). For decaying modes, we find $\pi < \chi < \frac{3}{2}\pi$, so the coarse grains concentrate on the stoss side. However, decaying modes are not relevant as they do not dominate the dynamics.

[39] The $L_{a0} = 0$ approximation, as proposed by *Walgreen et al.* [2004], is only justified when $L_{a0} \ll H$, provided that $ikS\langle \boldsymbol{q}_{b0,x}^{ref}\rangle$ in equation (13) is not small. The latter condition can be violated due to the mode considered (small k), the sediment properties ($S \approx 0$) and a small degree of asymmetry. For this last situation, Figure 4 shows the importance of using the full solution instead of the instantaneously adapting $L_{a0} = 0$ approximation. Indeed, the latter erroneously gives $\chi = \frac{1}{2}\pi$ (coarse grains concentrated on the lee side), whereas for symmetrical conditions $\chi = 0$ must hold (coarse grains at the crest).

3.5. Sensitivity to Physical Parameters

[40] Now we discuss the sensitivity of the results to the various physical parameters. As shown in Table 2, we define three tidal conditions: I (symmetric), II, and III (both asymmetric). As noted in section 2.2, combining large $\sigma_{\phi 0}$ with F_0^{co} values close to zero or one leads to unrealistically large differences in coarse and fine grain size. Therefore we will restrict our attention to bimodal mixtures for which

$$\phi^{fi} - \phi^{co} \leq 5, \qquad \text{i.e.} \qquad \frac{d^{co}}{d^{fi}} \leq 32. \tag{30}$$

This is the largest grain size range that can be covered within the sand regime [*Blott and Pye*, 2001], for which our model is designed to be valid. For a given $\sigma_{\phi 0}$, the constraint in equation (30) leads to lower and upper bounds for F_0^{co}; for a given F_0^{co} it leads to a maximum $\sigma_{\phi 0}$ value (marked by dots in Figures 5 and 6; see equation (A4) in Appendix A).

[41] For symmetrical conditions, Figure 5 shows the sensitivity of the (real-valued) relative growth rate ω/ω^{ref} to the parameters of the bimodal mixture (coarse grain fraction F^{co} and standard deviation $\sigma_{\phi 0}$) and the hiding power c_b. According to equation (25), this ratio equals P and since $P > 1$, it is seen that the hiding/exposure mechanism tends to enhance bank growth. For mixtures with a small content of coarse grains or a large standard deviation, this increase in growth rate is strongest (Figure 5). For increasing values of the hiding power c_b, it is seen that the growth rate increases, as well.

[42] For symmetric tidal conditions, the results show no sensitivity to the mean grain diameter d_{m0}, as this quantity does not enter the hiding/exposure formulation. This can be seen from the expressions for d^{co}/d_{m0} and d^{fi}/d_{m0} in Appendix A. The mean grain size, however, is likely to affect the value of the coefficient ν_b in the transport formula equation (6) and thus the (reference) timescale of bank growth and migration.

[43] In the asymmetric case, one should distinguish between the relative growth rate ω_r/ω_r^{ref} (Figure 6) and the relative migration rate ω_i/ω_i^{ref}. These quantities are again larger than one. However, compared to the symmetric case, the role of F_0^{co} and $F_0^{fi} = 1 - F_0^{co}$ turns out to be reversed. Now, for mixtures with a large content of coarse grains or a large standard deviation, the increase in growth rate is strongest (Figure 6). The asymmetric system shows a tendency to high values of ω_r/ω_r^{ref}, higher than the values obtained in the symmetric case.

[44] For most sediment mixtures, the value of S is negative (see equation (13)). However, sediment mixtures exist for which $S \geq 0$; for these mixtures the model shows a different behavior. When $S \approx 0$, ω_r/ω_r^{ref} attains large values. The full solution displays a peak, the height of which decreases for increasing L_{a0}, and the migration rate reverses with respect to the reference case of uniform sediment. The $L_{a0} = 0$ approximation is clearly not valid, as equation (28) collapses into an asymptote when S vanishes. The parameter

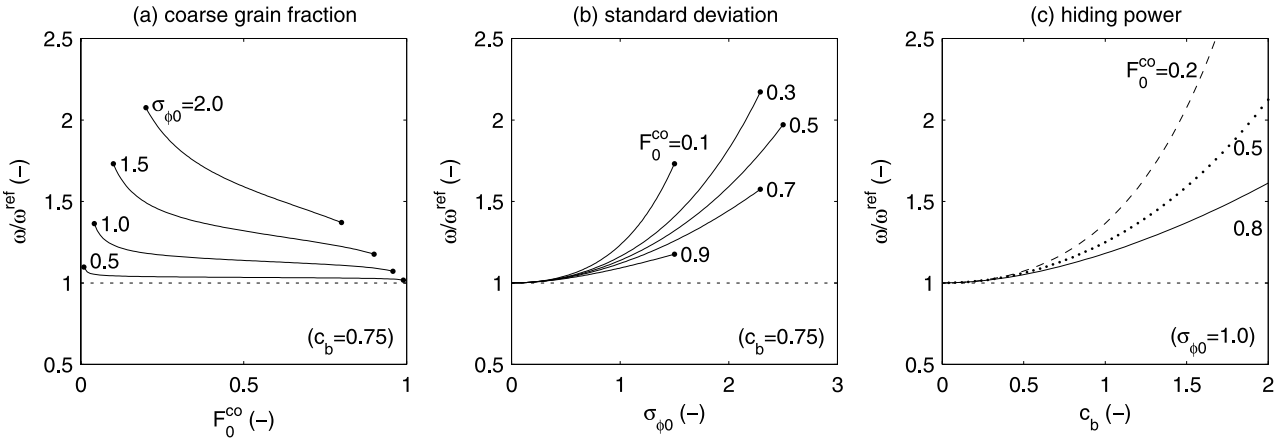

Figure 5. For symmetrical tidal conditions, sensitivity of relative growth rate $\omega/\omega^{\mathrm{ref}}$ to (a) the coarse-grain fraction F_0^{co}, (b) standard deviation $\sigma_{\phi 0}$, and (c) hiding power c_{b}. This has been done for different values of a second parameter (labeled curves), while fixing the third (see bottom right of each plot). In Figures 5a and 5b the dots indicate the boundary values of F_0^{co} and $\sigma_{\phi 0}$, respectively, for which $d^{\mathrm{co}}/d^{\mathrm{fi}} = 2^5$ (see text).

S becomes zero or positive when F_0^{co} is only slightly smaller than 1 and $c_{\mathrm{b}}\sigma_{\phi 0}$ is still large. To avoid extremely high values of $\omega_r/\omega_r^{\mathrm{ref}}$ in Figure 6, we used a lower value of the hiding power: $c_{\mathrm{b}} = 0.5$ instead of $c_{\mathrm{b}} = 0.75$.

4. Discussion

4.1. Physical Mechanisms

[45] Explaining the obtained spatial phase shifts between topography and grain size fraction is most straightforward in the case of a symmetrical tide. Then, a (nonmigrating) bank grows as a result of a tidally averaged sediment flux from trough to crest. Hiding/exposure is such that the transported sediment has a relatively high content of coarse grains, leading to a coarsening of the sediment at the crests and a fining in the troughs.

[46] In the asymmetrical case, where the system displays both growth and migration, the situation is less transparent. As the spatial phase shift is defined by the argument of the complex quantity $\xi = \hat{F}/\hat{h}$, we should focus on the dynamics of ξ, as given by equation (19). Assuming $\xi = 0$ at $t = 0$ and neglecting the terms proportional to ξ and ξ^2 on the right-hand side of equation (19), we find for small values of t:

$$\xi(t) \approx \frac{R\omega^{\mathrm{ref}} t}{L_{\mathrm{a0}}}. \tag{31}$$

For a growing mode ($\omega_r > 0$), migrating in the positive x direction ($\omega_i < 0$), this implies that $\chi = \arg(\bar{\xi}) > 0$. Hence there is an initial tendency for the peak in coarse grain fraction to shift toward the lee side of a growing and migrating bank. This tendency immediately stems from the fact that coarse material is transported more easily than fine material ($R > 0$).

[47] To account for the potential presence of small-scale sand ripples, the active layer thickness has been chosen of the order of a few centimeters. The detailed dependency of the ripple height on, for example, sediment properties does not require detailed specification. This is because the results from our linear stability model only involve the layer

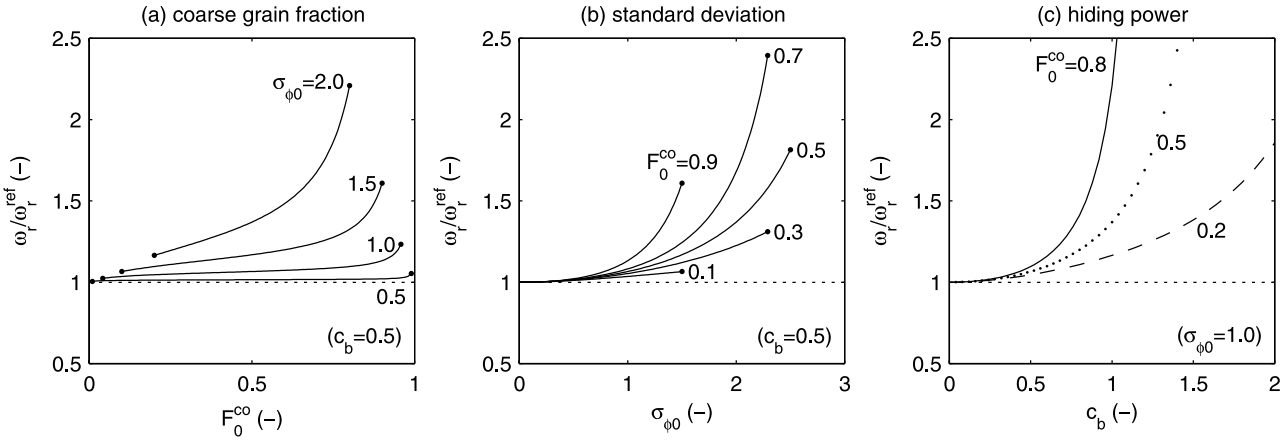

Figure 6. For asymmetrical tidal conditions (condition II in Table 2), sensitivity of relative growth rate $\omega_r/\omega_r^{\mathrm{ref}}$ to (a) F_0^{co}, (b) $\sigma_{\phi 0}$, and (c) c_{b}. For an explanation of the parameter values, see caption of Figure 5.

thickness L_{a0} and not its perturbation L_{a1} (see equations (13)–(17) in section 3.1).

4.2. Comparison with *Walgreen et al.* [2004]

[48] Both the present study and the work by *Walgreen et al.* [2004] follow a stability approach to investigate grain size variations over tidal sandbanks. The geometries of the two models, however, are essentially different (Figure 1).

[49] The model used by *Walgreen et al.* [2004] is an extension of the shelf model by *Calvete et al.* [2001], who considered uniform sediment. Characteristic of their geometry is the presence of an impermeable shoreface and a sloping inner shelf. In the basic state, the shelf slope is sustained by an up-shelf flux due to wave asymmetry, which is not explicitly modeled but assumed to balance the gravitational down-shelf sediment flux. For fair weather conditions, *Calvete et al.* [2001] find tidal sandbanks, both "trapped to the inner shelf" and on the outer shelf. In either case, these banks have a cyclonic bank orientation, strongly resembling the tidal sandbanks found in offshore models [*Huthnance*, 1982]. For tidally dominated conditions, neither the shoreface nor the shelf slope affects the morphodynamics crucially. However, solving for the cross-shore structure of the linear eigenvalue problem requires numerical techniques, making it more complicated than the purely sinusoidal structure found in the shore-parallel direction. *Walgreen et al.* [2004] did not investigate the cross-shore structure of the spatial phase shift χ.

[50] In our offshore model, both topography and spatial grain size variations are sinusoidal in the two horizontal directions. As a result, the spatial phase shift can be characterized by a single χ value. Despite the geometrical simplification, we do not find considerable differences with the results by *Walgreen et al.* [2004]. This implies that the presence of the shoreface and sloping inner shelf does not affect the properties of the sandbank system, i.e., neither bank dynamics nor grain size variations.

[51] We have presented a solution which unifies the results for symmetrical and asymmetrical tidal currents. The approximate results by *Walgreen et al.* [2004] (who took $L_{a0} = 0$ when interpreting the results) are thus extended into the limiting case of small tidal asymmetry (Figure 4).

4.3. Observations

[52] As noted in the Introduction, observations indicate that the coarsest grains are usually found either on the crests or on the lee side of the tidal sandbank (Table 1). This qualitatively agrees with the results from the present model for symmetrical and asymmetrical tidal conditions, respectively. Herein, we have used topography as an indication of symmetrical or asymmetrical conditions. In particular, we assume that the presence of a gentler stoss side and a steeper lee side are indicative of migration [*Dyer and Huntley*, 1999], and hence of asymmetric conditions, and hence of a nonzero value of the residual sediment flux $\langle q_{b0,x}^{ref} \rangle$.

[53] However, the presence of along-bank variations in both topography and sediment characteristics complicates the interpretation at certain locations. This applies for example to the "kink" in the Westhinder Bank, and the area between Sizewell Bank and Dunwich Bank. We feel that a quantitative comparison is beyond the scope of the present study. Such would require more detailed knowledge of grain size distributions.

5. Conclusion and Outlook

[54] We conclude that most of the observed grain size variations over tidal sandbanks (particularly on the Belgian continental shelf) can be explained by a dynamic hiding/exposure formulation within an active layer approach considering a bimodal sediment mixture. Coarse grains gather at the bank's crest (symmetrical tidal conditions) or on the lee side (asymmetrical conditions). The geometrical properties of the fastest growing mode (wavelength, orientation) are not affected by this model extension, although growth and migration rates increase with respect to the reference case of uniform sediment.

[55] Compared to our analysis, the more complicated geometrical features of an earlier model by *Walgreen et al.* [2004] (shoreface, sloping inner shelf) do not affect the growth and grain size variation properties of the sandbank system. In addition, we have shown that the $L_{a0} = 0$ approximation, as used by *Walgreen et al.* [2004] to analyze the model results, is not valid when tidal asymmetry is weak. An exact solution for the phase shift can readily be found, showing that the $L_{a0} = 0$ approximation overestimates the spatial phase shift.

[56] We followed a stability approach that assumes a small ratio of bank amplitude and water depth. A next step will be to investigate the active layer approach in the finite amplitude regime, i.e., when the above assumption of small perturbations is no longer valid. This requires a nonlinear model capable of describing tidal sandbanks in morphodynamic equilibrium [*Roos et al.*, 2004]. Such an approach leads to cross-sectional bank profiles that are no longer sinusoidal, introducing a relatively gentle stoss slope and a steeper lee side. A further suggestion is to investigate the grain size variations in a geometry that considers a finite bank length. This allows the study of possible grain size variations in the along-bank direction, for example toward the bank ends [*Pattiaratchi and Collins*, 1987; *Deleu et al.*, 2004].

Appendix A: Characterization of a Bimodal Sediment Mixture

[57] The bimodal sediment mixture can be fully characterized by three quantities: the average grain diameter, the standard deviation and the coarse grain fraction. To show this, let us consider the relations for mean value and standard deviation, given by

$$\mu_\phi = F^{co}\phi^{co} + F^{fi}\phi^{fi}, \tag{A1}$$

$$\sigma_\phi^2 = F^{co}\left(\phi^{co} - \mu_\phi\right)^2 + F^{fi}\left(\phi^{fi} - \mu_\phi\right)^2 = F^{co}F^{fi}\left(\phi^{fi} - \phi^{co}\right)^2, \tag{A2}$$

in which $F^{fi} = 1 - F^{co}$. Combining equations (A1) and (A2) leads to the following expressions for the coarse and fine grain diameters:

$$\frac{d^{co}}{d_{m0}} = 2^{\sigma_{\phi 0}\sqrt{\frac{1-F_0^{co}}{F_0^{co}}}}, \quad \frac{d^{fi}}{d_{m0}} = 2^{-\sigma_{\phi 0}\sqrt{\frac{F_0^{co}}{1-F_0^{co}}}}, \tag{A3}$$

respectively, here formulated in terms of the three quantities d_{m0}, $\sigma_{\phi 0}$ and F_0^{co}. We have added the subscript 0 to denote spatially invariant quantities that form the basis of the characterization. (The subsequent analysis introduces perturbations to d_m, σ_ϕ and F^{co} that are allowed to vary in space and time.) From equation (A3), it follows that the ratio of the coarse and fine grain diameters satisfies

$$\frac{d^{co}}{d^{fi}} = 2^{\frac{\sigma_{\phi 0}}{\sqrt{F_0^{co}F_0^{co}}}}. \tag{A4}$$

Appendix B: Details of the Solution Method

[58] The linearized hydrodynamic equations read

$$g\nabla\zeta_1 + \frac{\partial \boldsymbol{u}_1}{\partial t} + (\boldsymbol{u}_0\cdot\nabla)\boldsymbol{u}_1 + f\boldsymbol{e}_z\times\boldsymbol{u}_1 + \frac{r\boldsymbol{u}_1}{H} = -\frac{r\boldsymbol{u}_0 h_1}{H^2}, \tag{B1}$$

$$H(\nabla\cdot\boldsymbol{u}_1) = \nabla\cdot(\boldsymbol{u}_0 h_1). \tag{B2}$$

The solution procedure is as follows. For the three unknowns u_1, v_1 and ζ_1, a form similar to equation (11) is assumed. The corresponding amplitudes $\hat{u}$, $\hat{v}$ and $\hat{\zeta}$ are time-dependent, and we expand them in a Fourier series, i.e., $\hat{u} = \sum_{m=-M}^{M} U_m \exp(imt)$ with complex coefficients U_m and truncation number M ($\hat{v}$ and $\hat{\zeta}$ are expanded in a similar form). The unknown Fourier components are then obtained numerically.

[59] The first-order evolution equations for the seabed and the coarse grain fraction read

$$(1-p)\frac{\partial h_1}{\partial t} = -\nabla\cdot\left[\langle\boldsymbol{q}_{b1}^{co}\rangle + \langle\boldsymbol{q}_{b1}^{fi}\rangle\right], \tag{B3}$$

$$(1-p)L_{a0}\frac{\partial F_1^{co}}{\partial t} = -F_0^{fi}\nabla\cdot\langle\boldsymbol{q}_{b1}^{co}\rangle + F_0^{co}\nabla\cdot\langle\boldsymbol{q}_{b1}^{fi}\rangle. \tag{B4}$$

The former is the linearized version of equation (3) for two grain size fractions "co" and "fi," whereas the latter follows from back substitution of equation (3) in equation (2).

[60] The first-order sediment flux of the coarse grains is given by

$$q_{b1}^{co} = \left[F_1^{co}G_0^{co} + F_0^{co}G_1^{co}\right]q_{b0}^{ref} + F_0^{co}G_0^{co}q_{b1}^{ref}. \tag{B5}$$

For the fine grains a similar expression holds, where we note that $F_1^{fi} = -F_1^{co}$. Here the first-order hiding/exposure coefficients are given by

$$G_1^{co} = -TG_0^{co}F_1^{co}, \qquad G_1^{fi} = -TG_0^{fi}F_1^{co}, \tag{B6}$$

where

$$T = \frac{c_b\sigma_{\phi 0}\ln 2}{\sqrt{F_0^{co}F_0^{fi}}} > 0. \tag{B7}$$

The above shows that, if the coarse grain fraction locally increases, so does the mean diameter, which implies that exposure decreases locally and hiding increases locally, as specified in equation (5). This means that the hiding and exposure coefficients both decrease, so the perturbed quantities in equation (B7) are indeed negative.

[61] Finally, taking into account that $v_0 = 0$, we find that the first order reference flux is given by

$$\boldsymbol{q}_{b1}^{ref} = \nu_b\left[u_0^2(3u_1, v_1) - \lambda_b|u_0|^3\nabla h_1\right]. \tag{B8}$$

Here we note that u_0, u_1 and v_1 are time-dependent.On the basis of the first-order reference sediment flux as given in equation (B8), we find that the reference growth rate is given by

$$\omega^{ref} = \frac{-\nu_b}{1-p}\left[\frac{\langle u_0^2(3ik\hat{u} + i\ell\hat{v})\rangle}{\hat{h}} + \lambda_b\langle|u_0|^3\rangle|\boldsymbol{k}|^2\right]. \tag{B9}$$

Finally, the tidally averaged sediment flux induced by the basic flow follows from inserting the basic flow expression (9) in the transport formula (6) and taking the tidal average:

$$\langle\boldsymbol{q}_{b0,x}^{ref}\rangle = \nu_b U_{M_0}\left(U_{M_0}^2 + \frac{3}{2}U_{M_2}^2 + \frac{3}{2}U_{M_4}^2\right) + \frac{3}{4}\nu_b U_{M_2}^2 U_{M_4}\cos\beta. \tag{B10}$$

The y component of the lowest-order sediment flux is zero, because we have chosen the basic flow, see equation (9), to be parallel to the x axis.

Notation

c_b	power of dynamic hiding/exposure coefficient.
c_{mig}	migration rate of tidal sandbank.
$d^{(j)}$	grain size of fraction j.
d_m	mean grain size.
d_{ref}	reference grain size (1mm).
f	Coriolis parameter.
$F^{(j)}$	grain size fraction of fraction j.
$\hat{F}$	complex amplitude of perturbed coarse grain fraction.
g	gravitational acceleration.
$G^{(j)}$	dynamic hiding/exposure coefficient of fraction j.
H	mean water depth.
h	position of seabed level.
$\hat{h}$	complex amplitude of perturbed seabed.
i	imaginary unit, $i^2 = -1$.
j	dummy used to denote grain size fraction.
$\boldsymbol{k}$	topographic wave vector with components k and ℓ.
L_a	active layer thickness.
M	truncation number in tidal Fourier expansion.
n	dummy in tidal Fourier expansion.
P	coefficient in the set of first-order evolutions equations.
Q	coefficient in the set of first-order evolutions equations.
$\boldsymbol{q}_b^{(j)}$	bed load sediment flux of fraction j.
$\boldsymbol{q}_b^{ref}$	reference bed load sediment flux.
R	coefficient in the set of first-order evolutions equations.
r	linear bottom friction coefficient.
S	coefficient in the set of first-order evolutions equations.
T	coefficient in the set of first-order evolutions equations.
t	time.
U	maximum value of the depth-averaged flow velocity.
U_{M_0}	residual component of the basic flow.
U_{M_2}	M_2 component of the basic flow.
U_{M_4}	M_4 component of the basic flow.

U_m mth Fourier component of the perturbed flow velocity component.
$\boldsymbol{u}$ depth-averaged flow velocity vector with components u and v.
$\hat{u}$ complex amplitude of perturbed flow velocity component in the x direction.
$\hat{v}$ complex amplitude of perturbed flow velocity component in the y direction.
$\boldsymbol{x}$ horizontal coordinate vector with components x and y.
β temporal phase shift between M_2 and M_4 tidal velocity components.
ϕ phi-scale for grain sizes.
μ_ϕ mean phi-value.
ϵ expansion parameter.
ζ free surface elevation.
$\hat{\zeta}$ complex amplitude of perturbed free surface elevation.
θ latitude.
μ angular frequency of M_2 tide.
ν_b coefficient in sediment transport formula.
λ_b bed slope coefficient in sediment transport formula.
σ_ϕ standard deviation of grain size in terms of phi scale.
χ spatial phase shift between topography and coarse-grain fraction.
ψ system's state vector.
ξ complex, relative fraction amplitude.
ω growth rate.
Ω angular frequency of Earth's rotation.

Subscripts

0 basic state.
1 perturbed state.
r real part.
i imaginary part.
fgm fastest growing mode.

Superscripts

co coarse-grain fraction.
fi fine grain fraction.
ref reference situation.

[62] **Acknowledgments.** This research has been carried out within the EU projects HUMOR (contract EVK3-CT-2000-00037) and EUMARSAND. The project has been cosponsored by the Technology Foundation STW, the applied science division of NWO, and the technology program of the Dutch Ministry of Economic Affairs.

References

Blott, S. J., and K. Pye (2001), GRADISTAT: A grain size distribution and statistics package for the analysis of unconsolidated sediment, *Earth Surf. Processes Landforms*, *26*, 1237–1248, doi:10.1002/esp.261.

Calvete, D., M. Walgreen, H. E. De Swart, and A. Falqués (2001), A model for sand ridges on the shelf: Effect of tidal and steady currents, *J. Geophys. Res.*, *106*(C5), 9311–9326.

Deleu, S., V. Van Lancker, and G. Moerkerke (2004), Morphodynamic evolution of the kink of an offshore tidal sandbank: The Westhinder Bank (southern North Sea), *Cont. Shelf Res.*, *24*, 1587–1610, doi:10.1016/j.csr.2004.07.001.

De Vriend, H. J. (1990), Morphological processes in shallow tidal seas, in *Residual Currents and Long Term Transport, Coastal Estuarine Stud.*, vol. 38, edited by R. T. Cheng, pp. 276-301, Springer, New York.

Dodd, N., P. Blondeaux, D. Calvete, A. Falqués, H. E. De Swart, S. J. M. H. Hulscher, G. Rozynski, and G. Vittori (2003), Understanding coastal morphodynamics using stability methods, *J. Coastal Res.*, *19*, 849–865.

Dyer, K. R. (1986), *Coastal and Estuarine Sediment Dynamics*, John Wiley, Hoboken, N. J.

Dyer, K. R., and D. A. Huntley (1999), The origin, classification and modelling of sand banks and ridges, *Cont. Shelf Res.*, *19*, 1285–1330.

Gao, S., M. B. Collins, J. Lanckneus, G. De Moor, and V. Van Lancker (1994), Grain size trends associated with net sediment transport patterns: An example from the Belgian continental shelf, *Mar. Geol.*, *121*, 171–185.

Hastings, M. E., L. J. Poppe, J. C. Hathaway (2000), Surficial sediment database, in *USGS East-Coast Sediment Analysis: Procedures, Database, and Georeferenced Displays*, edited by L. J. Poppe and C. F. Polloni, *U.S. Geol. Surv. Open File Rep.* [CD-ROM], 00–358, chap. 2. (Available online at http://pubs.usgsgov/of/of00-358/)

Hirano, M. (1971), River bed degradation with armouring, *Trans. Jpn. Soc. Civ. Eng.*, *3*, 194–195.

Houthuys, R., A. Trentesaux, and P. De Wolf (1994), Storm influences on a tidal sandbank's surface (Middelkerke Bank, southern North Sea), *Mar. Geol.*, *121*, 23–41.

Hulscher, S. J. M. H., H. E. De Swart, and H. J. De Vriend (1993), The generation of offshore tidal sand banks and sand waves, *Cont. Shelf Res.*, *13*, 1183–1204.

Huthnance, J. M. (1982), On one mechanism forming linear sandbanks, *Estuarine Coastal Shelf Sci.*, *14*, 79–99.

Lees, B. J. (1983), The relationship of sediment transport rates and paths to sandbanks in a tidally dominated area off the coast of East Anglia, UK, *Sedimentology*, *30*, 461–484.

Pattiaratchi, C., and M. Collins (1987), Mechanisms for linear sandbank formation and maintenance in relation to dynamical oceanographic observations, *Prog. Oceanogr.*, *19*, 117–176.

Ribberink, J. S. (1987), Mathematical modelling of one-dimensional morphological changes in rivers with non-uniform sediment, Ph.D. thesis, Tech. Univ. Delft, Delft, Netherlands.

Roos, P. C., S J. M. H. Hulscher, M. A. F. Knaapen, and R. M. J. Van Damme (2004), The cross-sectional shape of tidal sandbanks: Modeling and observations, *J. Geophys. Res.*, *109*, F02003, doi:10.1029/2003JF000070.

Seminara, G. (1995), Effect of grain sorting on the formation of bedforms, *Appl. Mech. Rev.*, *48*(9), 549–563.

Trentesaux, A., A. Stolk, B. Tessier, and H. Chamley (1994), Surficial sedimentology of the Middelkerke Bank (southern North Sea), *Mar. Geol.*, *121*, 43–55.

Trentesaux, A., A. Stolk, and S. Berné (1999), Sedimentology and stratigraphy of a tidal sand bank in the southern North Sea, *Mar. Geol.*, *159*, 253–272.

Van Lancker, V. (1999), Sediment and morphodynamics of a siliciclastic near coastal area, in relation to hydrodynamical and meteorological conditions: Belgian continental shelf, Ph.D. thesis, Ghent Univ., Ghent, Belgium.

Van Lancker, V., S. Honeybun, and G. Moerkerke (2000), Sediment transport pathways in the Broers Bank–Westdiep coastal system: Preliminary coast, in *Marine Sandwave Dynamics*, edited by A. Trentesaux and T. Garlan, pp. 205–212, Univ. of Lille 1, Lille, France.

Walgreen, M., H. E. De Swart, and D. Calvete (2003), Effect of grain size sorting on the formation of shoreface-connected sand ridges, *J. Geophys. Res.*, *108*(C3), 3063, doi:10.1029/2002JC001435.

Walgreen, M., H. E. De Swart, and D. Calvete (2004), A model for grain-size sorting over tidal sand ridges, *Ocean Dyn.*, *54*, 374–384, doi:10.1007/s10236-003-0066-3.

Zimmerman, J. T. F. (1981), Dynamics, diffusion and geomorphological significance of tidal residual eddies, *Nature*, *290*, 549–555.

Zimmerman, J. T. F. (1982), On the Lorentz linearization of a quadratically damped forced oscillator, *Phys. Lett. A*, *89*, 123–124.

H. W. M. Hoeijmakers and N. P. Kruyt, Engineering Fluid Dynamics, Faculty of Engineering Technology, University of Twente, P.O. Box 217, NL-7500 AE Enschede, Netherlands. (h.w.m.hoeijmakers@utwente.nl; n.p.kruyt@utwente.nl)

S. J. M. H. Hulscher and P. C. Roos, Water Engineering and Management, Faculty of Engineering Technology, University of Twente, P.O. Box 217, NL-7500 AE Enschede, Netherlands. (s.j.m.h.hulscher@utwente.nl; p.c.roos@utwente.nl)

R. Wemmenhove, Computational Mechanics and Numerical Mathematics, Institute of Mathematics and Computing Science, University of Groningen, P.O. Box 800, NL-9700 AV Groningen, Netherlands. (r.wemmenhove@math.rug.nl)